Liquid-crystal based drift-free polarization modulators: Part II. Ultra-stable Stokes and Mueller polarimeters

Jean Rehbinder, Jean Dellinger, Briseis Varin, Marc Torzynski, Yoshitate Takakura, Christian Heinrich, Jihad Zallat

Research Article | Vol. 31, No. 6 / 13 Mar 2023 / Optics Express 10882
Optics EXPRESS

Liquid-crystal based drift-free polarization modulators: Part II. Ultra-stable Stokes and Mueller polarimeters

JEAN REHBINDER,* JEAN DELLINGER, BRISÉIS VARIN, MARC TORZYNSKI, YOSHITATE TAKAKURA, CHRISTIAN HEINRICH, AND JIHAD ZALLAT

Laboratoire ICube, Université de Strasbourg, Bd Sébastien Brant, 67412 Illkirch, France
**rehbinder@unistra.fr*

Abstract: We have previously reported a new design for drift-free liquid-crystal polarization modulators (LCMs) based on liquid-crystal variable retarders (LCVRs). Here, we study their performance on Stokes and Mueller polarimeters. LCMs have polarimetric responses similar to LCVRs and can be used as temperature-stable alternatives to many LCVR-based polarimeters. We have built an LCM-based polarization state analyzer (PSA) and compared its performance to an equivalent LCVR-based PSA. Our system parameters remained stable over a wide range of temperature, precisely from 25°C to 50°C. Accurate Stokes and Mueller measurements have been conducted, paving the way to calibration-free polarimeters for demanding applications.

1. Introduction

Polarization is a feature of light that appears to be very useful for numerous applications. In the field of material science, ellipsometry [1] for example is a well-established technique to characterize semi-conductor thin films, as accurate polarization control allows in situ monitoring of thin layer growth. More challenging applications include polarimetry for remote sensing [2], astronomy [3] and bio-medicine [4] since environmental factors cannot be easily controlled. In that context, robust polarimeters are required.

Over the years, many designs have been proposed [5] and new ideas continue to be developed (e.g. polarization-sensitive micro-patterned imaging polarimeters [6], fast Mueller polarimeters involving spectral encoding [7] or metasurface-based polarimeters [8], among others). Most imaging polarimeters are based on conventional detectors coupled with dynamic polarization optics that would sequentially modulate the polarization of light. To that end, a variety of devices have been proposed: rotating waveplates [9], Pockels cells [10], photoelastic modulators [11,12], liquid crystal modules (Liquid Crystal Variable Retarders (LCVRs) [13] or Ferroelectric Liquid Crystal cells (FLCs) [14,15]).

Liquid crystals are particularly well suited for polarimetric imaging and are widely used in the research community, as well as in commercial polarimeters. They allow total control of the polarization and are easily driven electronically. Without moving part, they avoid image wanderings or vibrations. Their fast switching times (of the order of 1-10 ms for LCVRs) are compatible with full characterization of polarimetric responses within seconds. At the same time, liquid crystals can maintain a sufficiently long polarization state for most applications when combined with CCD or CMOS cameras. Finally, the usability of LCVRs (available with various form factors, small footprint, and low driving voltage in the 1-10 V range) makes them ideal for portable or space-qualified instruments.

The major drawback of LCVR-based polarimeters is their temperature dependence. Consequently, frequent and complete calibration of the system [16] is necessary (for example before any measurement [17]) to sustain accurate measurements. It has to be done over the whole range

#480774 https://doi.org/10.1364/OE.480774
Journal © 2023 Received 16 Nov 2022; revised 23 Jan 2023; accepted 14 Feb 2023; published 10 Mar 2023

Optics EXPRESS

of temperature where the polarimeter operates [18]. However, the drift of the measurement matrix would still affect the precision and the comparability of measurements taken at different temperatures: the conditioning of the system may vary, as the noise distribution over the elements of the Mueller matrix may change [19][20]. Alternatively, an active temperature control of LCVR modules has been proposed [21]. Such a strategy poses several challenges: thermalization time, maintaining uniform temperature distribution over the entire LCVR, additional power consumption, etc.

In Part I of this work [22], we have introduced a new design for temperature-stable Liquid Crystal Modulators (LCM) that can replace LCVRs in any LCVR-based polarimeter. In this paper, we will assess such an LCM-based polarimeter. In section 2, we explore the conditions under which an optimal polarimeter can be built with LCMs, in particular by taking into account achievable delays. Section 3 exposes the experimental setup and methods of data analyses for an LCM-based polarization state analyzer (PSA). Experimental validation is presented in section 4 and discussed in section 5.

2. Polarimeters based on liquid crystal modulators

LCVRs are very versatile and flexible. They have been used in various polarimeters. In some cases, only one polarization state is considered in the contrast optimization process for a given scene [23]. To determine the complete Stokes vector of an incoming light, at least four different samplings are required, and in the case of active polarimetry, a total of 4×4 measurements are necessary to retrieve the Mueller matrix of a sample (four polarization states for the illumination and four for the outgoing waves).

Here we explore the performance of LCM-based polarimeters, namely full Stokes and Mueller polarimeters, as compared to their LCVR-based counterparts.

2.1. LCMs as temperature-stable alternative to LCVRs

In this section, we recall the main results of Part I of this work [22], where we have shown that an LCM has the same polarimetric response as a conventional LCVR, except for the temperature-dependent retardance drift.

LCVRs act as continuously variable retarders with fixed eigen-axes. If we note $\varphi(T,V)$ the retardance of an LCVR for a given temperature-voltage couple (T, V), and T_0 the operating temperature it has been designed for, we have established that the response of the LCVR would only depend on a single parameter α according to:

$$\varphi(T, V) = \varphi_{T_0}(V) + \alpha\varphi_{T_0}(V)(T - T_0) \tag{1}$$

hence, the higher the operating retardance at T_0, the greater its rate of change with temperature.

The LCMs are built by stacking together two LCVRs ($LCVR_A$ and $LCVR_B$) with their eigen-axes perpendicular to each other. We have shown that with this configuration the retardance of the LCM is equal to $\varphi_{LCM} = \varphi_A - \varphi_B$. Parameter α varies from one LCVR to the next, allowing a mutual compensation of the temperature drift of $LCVR_A$ and $LCVR_B$. Temperature-stable operation of the LCM happens at calibrated voltage couples. Conversely, the compensation can be virtually switched off when φ_B is set to zero (see also Fig. S1 in the Supplement 1). Then the temperature dependence becomes negligible compared to the variations in retardance of $LCVR_A$.

In our previous work, we have also established that the LCMs would have reduced retardance range as compared to LCVRs mounted in the compensated modules. In the following, we show that LCMs can be used as a temperature-stable replacement of LCVRs in any LCVR-based polarimeter.

Optics EXPRESS

2.2. Conventional LCVR-based Stokes and Mueller polarimeters

In LCVR-based polarimeters, LCVRs usually act as electronically controlled polarization state selectors. For Stokes polarimetry, the compound LCVR-polarizer-sensor is generally referred to as Polarization State Analyser (PSA). As for Mueller polarimeters, a polarizer-LCVR stack is inserted in front of the illumination and is called a Polarization State Generator (PSG).

A standard configuration for a PSA (or reciprocally for a PSG) is the combination of a linear polarizer, an LCVR ($LCVR_1$) with its eigen-axis at 45° with respect to the polarizer axis, followed by a second LCVR ($LCVR_2$) with its eigen-axis parallel to the polarizer axis. Such a configuration permits to attain any pure polarization state on the Poincaré sphere. The analyzed (resp. generated) Stokes vector is expressed as [24,25] :

$$S = \begin{bmatrix} 1 & \cos(\varphi_1) & \sin(\varphi_2)\sin(\varphi_1) & \cos(\varphi_2)\sin(\varphi_1) \end{bmatrix}^T \tag{2}$$

where $\varphi_{1,2}$ is the retardance of $LCVR_{1,2}$ respectively. On the Poincaré sphere, a retarder acts as a rotator around the Stokes vector identifying its eigen-axis, with a rotation angle equal to its retardance. This is illustrated in Fig. 1.a) for the case $\varphi_1 = \varphi_2 = 120°$. The initial polarization corresponds to a horizontal linear polarization $S = [1\ 1\ 0\ 0]^T$ (Point P_A in Fig. 1.a). After interacting with $LCVR_1$, the polarization state is rotated along the larger dotted circle towards $S = [1\ -0.5\ 0\ \sqrt{3}/2]^T$ (Point P_B in Fig. 1.a). With $LCVR_2$, the polarization state is rotated along the smaller dotted circle to position $S = [1\ -0.5\ 0.75\ -\sqrt{3}/4]^T$ (Point P_C in Fig. 1.a). The whole trajectory P_A-P_B-P_C on the Poincaré sphere is represented by a solid blue line.

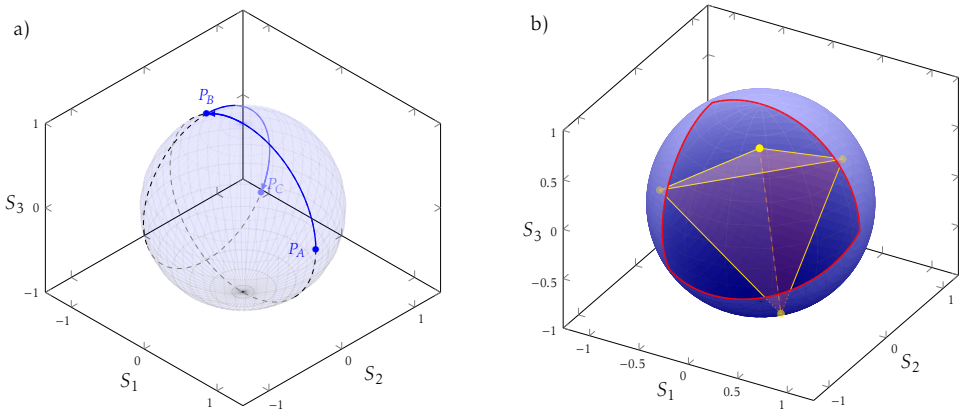

Fig. 1. Well-conditioned measurement matrix involving LCMs with limited retardance range. a) Trajectory on the Poincaré sphere as light travels across a PSG (blue line). The dotted lines represent the intersection of the Poincaré sphere with the planes where $LCVR_1$ and $LCVR_2$ operate their respective rotations. The starting point is at $S = [1\ 1\ 0\ 0]^T$. In the represented example: $\varphi_1 = \varphi_2 = 120°$. b) In red, boundary of the area that can be explored with retardance range of [0° 240°] for both LCMs. In this case, measurement matrix with ideal condition number ($\kappa(A) = \sqrt{3}$) is obtained. The inscribed tetrahedron permits to visualize one such matrix A.

For a Stokes- (or a Mueller-) polarimeter, 4 (or $4 \times 4 = 16$) intensity measurements have to be performed with different PSA states (or PSG and PSA). If we note A the 4×4 matrix obtained by stacking the 4 Stokes vectors set with the PSA, the Stokes vector S of the light to be analyzed may be deduced from the measured vector I according to:

$$S = A^{-1} I \tag{3}$$

Optics EXPRESS

The condition number of A (noted $\kappa(A)$) is frequently used as a figure of merit for polarimeters, as it quantifies the error propagation across the system [20,26–28]. The theoretical lower limit for such a number in the case of an ideal PSA is $\sqrt{3}$. It is obtained when the 4 probing Stokes vectors form a regular tetrahedron within the Poincaré sphere [29].

2.3. Stokes and Mueller polarimeters based on compensated modulators

LCM-based polarimeters have been built according to the same scheme. However, if both LCMs forming a PSA have retardance ranging less than 360°, some areas of the Poincaré sphere would not be reached (however, if one of the LCMs ranges up to 360° or more, it is sufficient for the second one to span 180° for any polarization state to be attained). It is worth mentioning that even in that case, ideal systems, i.e., systems with best conditioned A-matrix, can still be obtained. This is illustrated in Fig. 1.b) where retardance of both LCMs ranges from $\varphi_{min} = 0°$ to $\varphi_{max} = 240°$. Accessible polarization states on the Poincaré sphere are colored in blue, which entails that a large area of the sphere (enclosed by the red line) is not accessible. It is still possible to select 4 Stokes vectors forming a regular tetrahedron, one solution being provided by the four yellow points within the blue zone (see Fig. 1.b).

To start with, we look for the minimum range needed to obtain an optimal $\kappa(A)$. To that end, we perform a calculation by imposing the minimal retardance to $\varphi_{min} = 0°$ for both LCMs, and by varying the highest temperature-compensated retardance φ_{max} for each LCM. A constrained optimization (using *fmincon* in MATLAB R2016b) on the condition number of A has been performed, with the retardance of each LCM maintained within the range $[\varphi_{min}, \varphi_{max}]$. Figure 2 shows a map of the lowest condition number as a function of φ_{max} for both LCMs. The theoretical limit for the best achievable $\kappa(A)$ has been achieved, even for limited ranges. A higher range for one of the LCMs allows to relax the constraints on the other. For example, if the first LCM (φ_A) has a range of 360° or more, the second (φ_B) one may have retardance as low as 90°. If both LCMs sweep within the same range, φ_{max} must be higher than 212° so as to reach the optimum. In practice, when building LCM-based polarimeters, a trade-off between thermal stability and condition number is needed. Indeed for low noise data, it would still be possible to obtain fine polarimetric measurements with non-optimal $\kappa(A)$ [15].

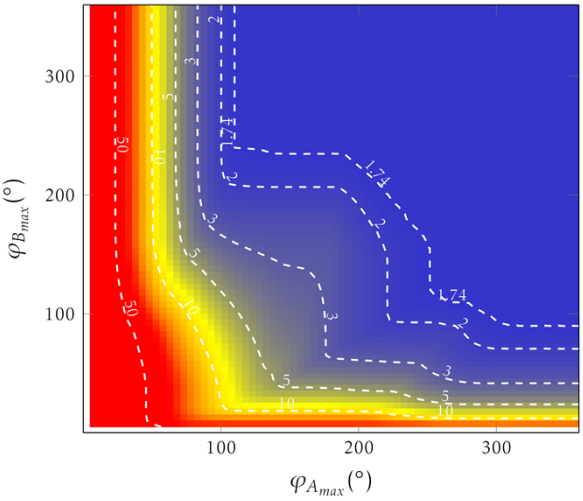

Fig. 2. Map for condition number. Contour plot of lowest $\kappa(A)$. attainable as a function of the retardance range of $LCVR_A$ ($[0° \varphi^A{}_{max}]$) and $LCVR_B$ ($[0° \varphi^B{}_{max}]$).

Optics EXPRESS

3. Materials and methods

In order to investigate the performance of an LCM-based polarimeter, we have performed polarimetric measurements with varying temperatures. To that end, we have mounted a temperature-stable PSA by combining two home-built LCMs and conducted experiments in a temperature controlled enclosure.

3.1. Setup

Our setup is shown in Fig. 3. It corresponds to a Mueller polarimeter. The light source is a fiber-guided halogen lamp (Dolan-Jenner MI 150) collimated with an objective (Avenir TV zoom lens 75 mm, f/22) and filtered around 600 nm by means of a bandpass filter (50 nm FWHM, Edmund Optics #84-797).

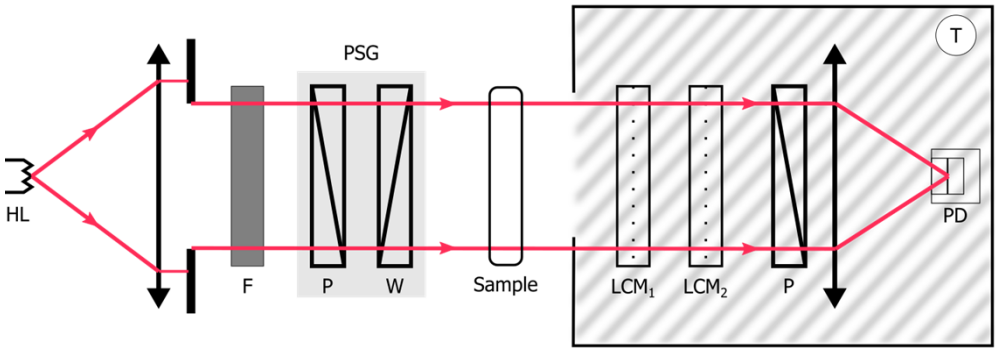

Fig. 3. Schematic of the optical setup. F: dichroic filter, P: polarizer, W: rotating waveplate, PD: detector. The hatched box represents the temperature controlled enclosure

The PSG is based on a rotating waveplate ($\lambda/4$ at 632.8 nm, Newport, 20RP34). It is combined with a polarizer (Newport, 20LP-VIS) positioned upstream towards the illumination. The waveplate generates a retardance of 96.4° at the operating wavelength (600 nm). It is sequentially set at four angles: -51.69°, -15.12°, 15.12°, 51.69°, which permits to generate an optimized set of 4 incoming polarization states [20,30]. For such a configuration, the measurement matrix W has a condition number of $\kappa(W) = 3.07$.

The light then interacts with the sample and is subsequently analyzed with the LCM-based PSA. The latter will be described in detail in the next section. Behind the PSA, a lens (f = 35 mm, Thorlabs) concentrates the outgoing light onto a single-channel silicon detector (PDA 100A2 Thorlabs). The PSA and the detector are assembled in a heated enclosure which is thermally isolated. It also includes a fan insuring rapid homogenization of the air within the close. Temperatures of the LCVRs are continually monitored by sensors inserted in their mount.

3.2. LCM-based polarimeter

Two home-built LCMs have been assembled according to the procedure described in Part I of this work [22]. Briefly, each LCM consists of two commercially available LCVRs (Meadowlark, LRC 300 VIS) mounted in a metal holder with their eigen-axes perpendicular to each other. The LCMs are calibrated within a heated enclosure similar to the one described above. Such a calibration would determine their operating points, i.e., the pairs of voltage for which thermal drift of the LCVRs would mutually compensate.

For validation purposes, we have conducted experimentations on an LCM-based PSA. It has the conventional architecture of LCVR-based polarimeters as described in section 2.2, namely a linear polarizer (on the detector side) followed by two LCMs. With respect to the laboratory

Optics EXPRESS

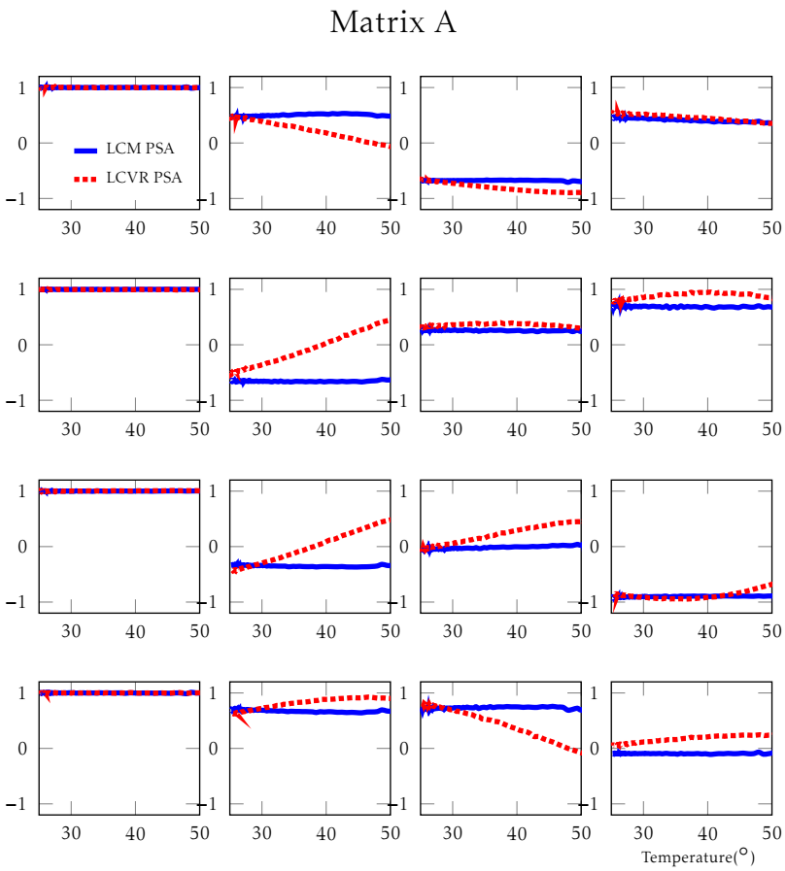

Fig. 4. Temperature dependence of the measurement matrix A of a PSA with compensation (LCM-PSA, blue line) and without compensation (LCVR-PSA, red line).

frame, the axis of the polarizer and those of the first and second LCMs are set to 0°, 45° and 0° respectively.

Based on the previous retardance calibration, four projecting polarization states have been chosen for the PSA. The corresponding Stokes vectors were then stacked in a 4×4 matrix A. The retardance of the first LCM would range from -250° to -12° for a temperature stable operation. As for the second, the range was [4° 210°]. An optimized configuration of the PSA has been sought by means of a constrained optimization procedure such as the one described in section 2.3.

3.3. *Polarimetric measurements with a compensated PSA*

The combination of the rotating PSG and the LCM-based PSA would form a Mueller polarimeter. It will be used to retrieve the Mueller matrix of a pure element such as a waveplate. By combining two-by-two the polarization states chosen for the PSG (matrix W) and those for the PSA (matrix A), the 4×4 intensity matrix B would satisfy:

$$B = AM_{WP}W \tag{4}$$

where M_{WP} is the Mueller matrix of the waveplate. The experimental setup permits to observe the temperature dependent behavior of the measurement matrix A, as well as the impact of the temperature fluctuations on the measure M_{WP}. At room temperature T_0, the measurements

Optics EXPRESS

matrices $A(T_0)$ and $W(T_0)$ were determined by means of the Eigenvalues Calibration Method (ECM) [16]. After calibration, the Mueller matrix M_{WP} of the waveplate is measured. Since the waveplate and the PSG are set outside of the heated enclosure, M_{WP} and W are considered temperature independent.

M_{WP} being the Mueller matrix of a retarder, is invertible (even unitary). By setting the temperature in the enclosure to T, $A(T)$ is determined by inverting Eq. (4):

$$A(T) = B(T)W^{-1}M_{WP}^{-1} \tag{5}$$

By noting M'_{WP} the Mueller matrix retrieved thanks to the measurement matrices calibrated at room temperature, thermal effects may be investigated by comparing such a matrix to M_{WP}, as it satisfies:

$$M'_{WP} = A(T_0)^{-1}B(T)W^{-1} \tag{6}$$

M'_{WP} represents the Mueller matrix that would be obtained when using a polarimeter calibrated at room temperature. Since the Mueller matrix of the waveplate does not depend on temperature, M'_{WP} is indicative of measurement errors due to temperature induced changes in the system. In a temperature-stable system, however, $A(T)$ remain constant and equal to $A(T_0)$ and $M_{WP} = M'_{WP}$ at any given temperature.

4. Results

The setup exhibited in the previous section has been used to expose the benefits of LCMs over LCVRs. The first investigation has been conducted on the response of the system itself when varying the temperature. With the same setup, we have also monitored the impact of thermal stabilization on polarimetric measurements, should it be for Stokes or Mueller polarimeters.

4.1. Measurement matrix of a compensated PSA

Although the temperature dependence of a single LCVR can be summarized by a simple equation (Eq. (1)), in an LCVR-based polarimeter the temperature dependence can be quite complex. A Mueller polarimeter, for example, involves 4 LCVRs (two for the PSG and two for the PSA), with each LCVR operating at 4 different voltages. The retardance drifts are module dependent as well as voltage dependent, and the final matrix $A(T)$ will be significantly impacted by the coalescence of all the parameters.

In the following experiments, we will be focusing on the temperature dependence of a PSA only. This means considering a Stokes-meter, i.e., a polarimeter analyzing light incoming (without control over the illuminating polarization). The temperature dependent matrix $A(T)$ related to the LCM-based PSA has been measured according to the procedure described in section 3.3. To that end, two sets of voltages have been considered. The "LCM-PSA" optimized voltage set has been chosen in such a way as to compensate temperature dependence. The "LCVR-PSA" voltage set simulates an LCVR-based system. The latter has been obtained by imposing $\varphi_B = 0$ for both LCMs (see section 2.1). As for LCM-PSA, the corresponding four Stokes vectors are adjusted with retardances accessible with both LCMs. In the LCVR-PSA situation, only $LCVR_A$ of each LCM will be used to sweep through retardances, so that the A-matrices are equal at 25°C. The evolution of matrix A for both LCM-PSA and LCVR-PSA are compared in Fig. 4, with temperature ranging from 25°C to 50°C. In the absence of compensation, the elements of A_{LCVR} undergo very significant shifts: for example, $A_{2,2}$ varies from -0.52 at 25°C to 0.45 (almost 50% of the total range for this element) at 50°C. Not all elements are affected in the same way. In the current situation, $A_{1,4}$ and $A_{2,3}$ for example are almost constant over the considered temperature range. Such behaviors can be explained by several factors: a) firstly, by the fact that the temperature dependence is stronger when the retardance is high, b) secondly, by the nonlinear dependence of the elements on the retardance (see Eq. (1) in section 2.1), c) finally, by a possible

Optics EXPRESS

mutual compensation of the drift effects by the first and second LCM (especially for the fourth column of A).

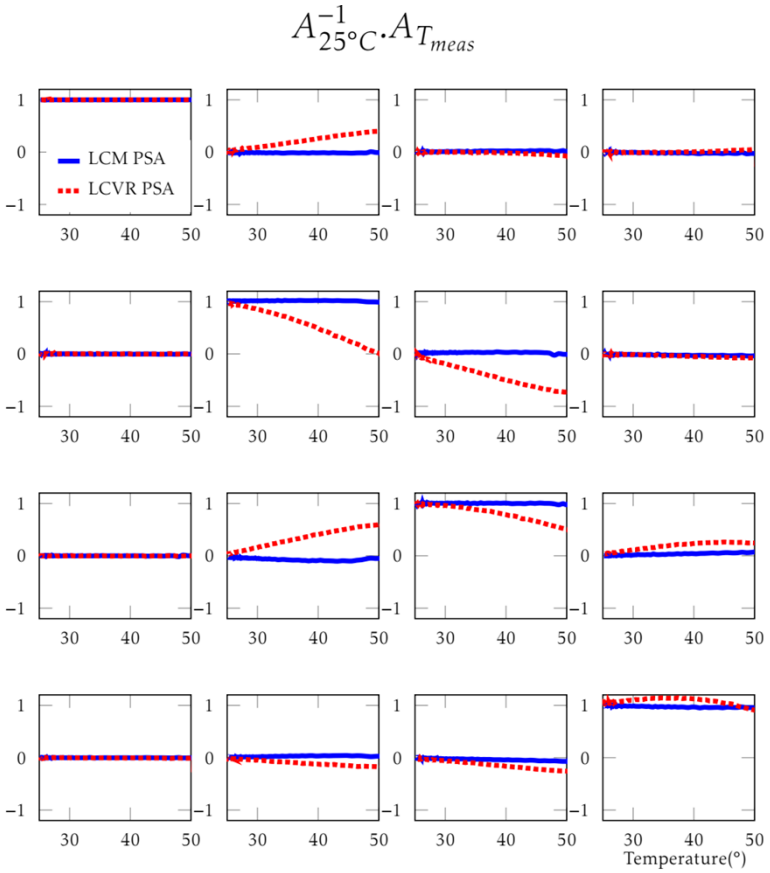

Fig. 5. Temperature dependence of the transfer matrix $A_{25°C}{}^{-1}A_{Tmeas}$ of a PSA with compensation (LCM-PSA, blue line) and without compensation (LCVR-PSA, red dotted line).

LCM-PSA exhibits a much more stable A-matrix. We observe variations limited to 0.1 over the whole range of temperature. In our experiments, perfect compensation of the temperature-drift has not been achieved. A small mismatch has been observed on the derivatives of the retardance curves of the LCVRs forming each LCM. Such a residual mismatch appears to be the limiting factor for achieving even better stabilization of matrix A.

4.2. Stokes parameters

Relating the perturbations affecting matrix A to the errors propagated in the retrieved Stokes vector is not straightforward. In practice, the measurement errors of the polarimeter will depend on the polarization itself. To better support our argument, we have calculated the product of the inverted PSA matrix obtained at room temperature and the PSA matrix at the operating temperature T, i.e, $A_{25°C}{}^{-1}A_{Tmeas}$. It corresponds to the transition matrix between the real Stokes vector S and the measured Stokes vector S_{meas}. Indeed:

$$S_{meas} = A(T_0)^{-1} I_{meas} = A(T_0)^{-1} A(T) S \tag{7}$$

Optics EXPRESS

In a well-calibrated system, the transition matrix is equal to the identity. Deviations of the *(i,j)*-element of such a matrix from the expected value are significant of the impact of the temperature on the *i*-th element of S_{meas}, provided the *j*-th element of *S*.

The behavior of $A_{25°C}{}^{-1}A_{Tmeas}$ between 25°C and 50°C is shown in Fig. 5 for both systems (LCVR-PSA and LCM-PSA). Again, for LCVR-PSA, deviations are significant from the expected identity matrix. The second element on the diagonal drops from 1 to almost 0 at 50°C while some off-diagonal elements surpass 0.5. In the current case, S^0 and S^3 remain relatively unaffected by perturbations, conversely S^1 and S^2 are very sensitive to temperature-drift.

For illustration purpose, Table 1 shows the results obtained as measurements were made at 30°C and calibration performed at 25°C. Here, the incoming Stokes vector is $S_{real} = [1\ 0\ 1\ 0]^T$. In the LCM-PSA configuration, the transfer matrix $A_{25°C}{}^{-1}A_{Tmeas}$ remains stable within 0.1 for all elements, over the whole temperature range. An improvement of one order of magnitude for S^2 may be observed.

Table 1. Measurement errors at 30℃ for a system calibrated at 25℃

S_{real}	S_{meas} LCVR	S_{meas} LCM
1	1.002	1.010
0	-0.182	0.027
1	0.959	1.002
0	-0.057	-0.022

4.3. Mueller matrices

The performance of the LCMs inserted in a Mueller polarimeter has been investigated by retrieving the Mueller matrix of a waveplate under temperature stabilization or not, and by extracting the physical characteristics of the optical element. Again, the calibration matrix $A_{25°C}$ obtained at 25°C has been used for the measurements made over the entire range of temperature. It is worth noting that only the PSA is located in the heated enclosure. The PSG with the rotating waveplate remained at room temperature during the whole experiment. Once the Mueller matrix obtained (by applying Eq. (6)), its polar decomposition has been carried out according to an adapted version of the Lu and Chipman approach [31,32]. Such an algorithm allows to extract fundamental polarimetric properties (retardance, diattenuation, depolarization) from the Mueller matrix. The variations of the retardance, orientation of the retarder, diattenuation and depolarization are shown in Fig. 6 a), b), c) and d) respectively. At room temperature, a retardance of 127° and an orientation of 33° were obtained. As expected for a waveplate, the diattenuation and depolarization were close to 0.

The measured retardance remained stable for both LCVR- and LCM-PSA from 25°C to about 35°C, where the retardance measured with the LCVR-PSA started to deviate quickly. At 50°C, the error on the retardance reached 14° for the LCVRs and was limited to 3° for the LCMs. The orientation of the waveplate was more sensitive to temperature changes. With the LCVR-PSA, the values drifted continuously up to 46° at 50°C while with the LCM-PSA, deviations were 1° at the most from the expected value of 33°.

The drift of the measurement matrix for the LCVR-PSA can also be associated with the appearance of anomalous diattenuation and depolarization as temperature increases. The diattenuation features an almost linear dependence on temperature and reaches 0.43 at 50°C. The depolarization increases more slowly to attain 0.13 at 50°C. For LCM-PSA, these anomalies remain close to 0. A residual increase of the parameters may however be observed: it is limited to 0.03 for diattenuation and 0.027 for depolarization.

Optics EXPRESS

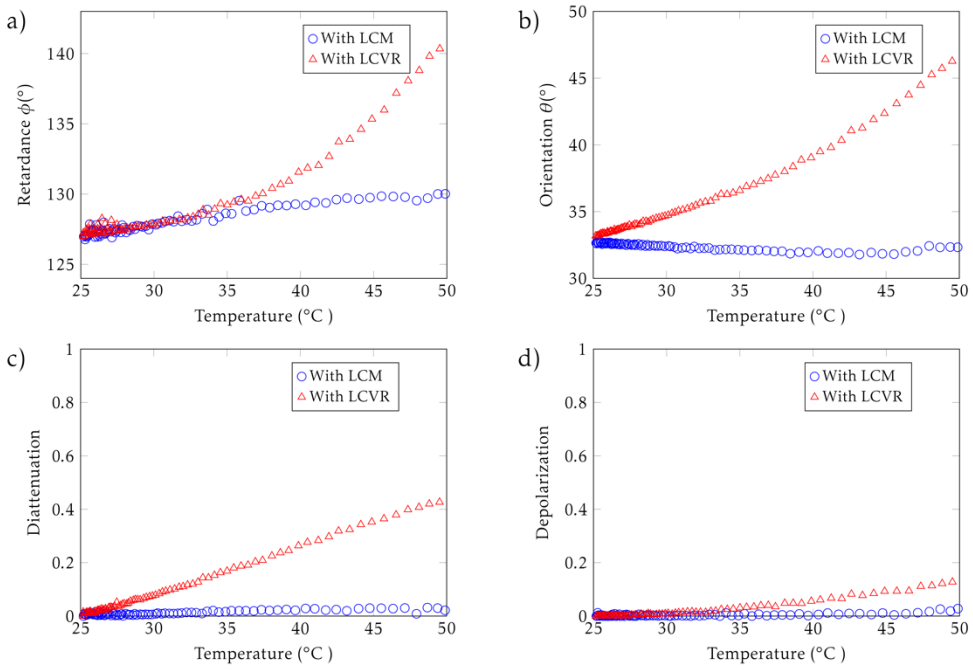

Fig. 6. Temperature dependent parameters of a waveplate obtained with compensated (LCM-PSA) and standard (LCVR-PSA) PSA in the Mueller configuration: (a) Retardance, (b) orientation of the retarder, (c) Diattenuation, and (d) Depolarization extracted from the Mueller matrix using polar decomposition [31,32].

5. Discussion and conclusion

In this part of our work on drift-free LCMs, we have shown that such modulators may be considered as interesting alternatives to LCVRs for polarimeters. To that end, we have demonstrated that the limited retardance-range of LCMs is not an obstacle for mounting polarimeters with optimal performances. We have then built and tested such an LCM-based polarimeter. At room temperature, the device has the same characteristics (condition number, low operating voltages, small footprint. . .) as an LCVR-based polarimeter. As the temperature changes, the LCM is by far more robust in terms of stability. This has been established for both the instrumental measurement matrix and polarimetric (Stokes and Mueller) assessments.

With further developments, the retardation range may be extended. This could be achieved either by carefully selecting the LCVR pair forming the LCM or by developing liquid crystals especially optimized for such a purpose. As on the limits of achievable condition number, our study may also apply to LCVRs with limited retardance range, which could occur at certain wavelengths, or for LCVRs optimized for fast switching times.

The current investigations have proven that LCM-based polarimeters are capable of providing reliable measurements over a wide range of temperature. Even more accurate measurements could be achieved by taking into account the residual retardance-drifts by assessing beforehand the temperature response of the polarimeter to be employed.

To conclude, our system corrects the main shortcoming of LCVRs, which otherwise are excellent modulators for polarimetry. The stability of an LCM-based instrument should permit to drastically reduce the amount of calibration procedures. It would also produce stable measurements in unsteady thermal environments. Obvious fields of application of this new

Optics EXPRESS

device would be biomedical polarimetry and astronomy. Such an instrument is currently being used by our team in a clinical trial for imaging skin lesions.

Funding. Société d'Accélération du Transfert de Technologies (Conectus Alsace, Dermapol project).

Disclosures. JZ, MT and CH (P).
The authors declare that there are no conflicts of interest

Data availability. Data sustaining the results presented in this paper are not publicly available at this point but may be obtained from the authors upon reasonable request

Supplemental document. See Supplement 1 for supporting content.

References

1. H. Tompkins and E. A. Irene, *Handbook of Ellipsometry* (William Andrew, 2005).
2. J. S. Tyo, D. L. Goldstein, D. B. Chenault, and J. A. Shaw, "Review of passive imaging polarimetry for remote sensing applications," Appl. Opt. **45**(22), 5453–5469 (2006).
3. J. Tinbergen, *Astronomical Polarimetry* (Cambridge University Press, 1996).
4. N. Ghosh and A. I. Vitkin, "Tissue polarimetry: concepts, challenges, applications, and outlook," J. Biomed. Opt. **16**(11), 110801 (2011).
5. F. Snik, J. Craven-Jones, M. Escuti, S. Fineschi, D. Harrington, A. De Martino, D. Mawet, J. Riedi, and J. S. Tyo, "An overview of polarimetric sensing techniques and technology with applications to different research fields," **9099**, 90990B–67 (2014).
6. W.-L. Hsu, G. Myhre, and K. Balakrishnan, *et al.*, "Full-Stokes imaging polarimeter using an array of elliptical polarizer," Opt. Express **22**(3), 3063–3074 (2014).
7. S. Rivet, M. Dubreuil, A. Bradu, and Y. Le Grand, "Fast spectrally encoded Mueller optical scanning microscopy," Sci. Rep. **9**(1), 3972 (2019).
8. F. Ding, Y. Chen, and S. I. Bozhevolnyi, "Metasurface-Based Polarimeters," Appl. Sci. **8**(4), 594 (2018).
9. R. M. A. Azzam, "Photopolarimeter using two modulated optical rotators," Opt. Lett. **1**(5), 181–183 (1977).
10. R. C. Thompson, J. R. Bottiger, and E. S. Fry, "Measurement of polarized light interactions via the Mueller matrix," Appl. Opt. **19**(8), 1323 (1980).
11. E. Compain and B. Drevillon, "High-frequency modulation of the four states of polarization of light with a single phase modulator," Rev. Sci. Instrum. **69**(4), 1574–1580 (1998).
12. S. Alali, A. Gribble, and I. Alex Vitkin, "Rapid wide-field Mueller matrix polarimetry imaging based on four photoelastic modulators with no moving parts," Opt. Lett. **41**(5), 1038 (2016).
13. J. M. Bueno and P. Artal, "Double-pass imaging polarimetry in the human eye," Opt. Lett. **24**(1), 64 (1999).
14. . E. Garcia-Caurel, A. De Martino, and B. Drévillon, "Spectroscopic Mueller polarimeter based on liquid crystal devices," Thin Solid Films **455-456**, 120–123 (2004).
15. A. Lindberg, J. Vizet, J. Rehbinder, C. Gennet, J.-C. Vanel, and A. Pierangelo, "Innovative integrated numerical-experimental method for high-performance multispectral Mueller polarimeters based on ferroelectric liquid crystals," Appl. Opt. **58**(19), 5187–5199 (2019).
16. E. Compain, S. Poirier, and B. Drevillon, "General and self-consistent method for the calibration of polarization modulators, polarimeters, and Mueller-matrix ellipsometers," Appl. Opt. **38**(16), 3490 (1999).
17. J. M. Bueno, "Polarimetry using liquid-crystal variable retarders: Theory and calibration," J. Opt. A: Pure Appl. Opt. **2**(3), 216–222 (2000).
18. J. S. Baba and P. R. Boudreaux, "Wavelength, temperature, and voltage dependent calibration of a nematic liquid crystal multispectral polarization generating device," Appl. Opt. **46**(22), 5539–5544 (2007).
19. F. Goudail, "Noise minimization and equalization for Stokes polarimeters in the presence of signal-dependent Poisson shot noise," Opt. Lett. **34**(5), 647 (2009).
20. J. Zallat, S. Aïnouz, and M. P. Stoll, "Optimal configurations for imaging polarimeters: Impact of image noise and systematic errors," J. Opt. A: Pure Appl. Opt. **8**(9), 807–814 (2006).
21. M. Silva-López, L. Bastide, R. Restrepo, P. García Parejo, and A. Álvarez-Herrero, "Evaluation of a liquid crystal based polarization modulator for a space mission thermal environment," Sens. Actuators, A **266**, 247–257 (2017).
22. J. Rehbinder, J. Dellinger, C. Heinrich, J. Zallat, M. Torzynski, B. Varin, and Y. Takakura, "Liquid-crystal based drift-free polarization modulators: Part I. Design and operation," Opt. Express **30**(9), 14966–14977 (2022).
23. G. Anna, H. Sauer, F. Goudail, and D. Dolfi, "Fully tunable active polarization imager for contrast enhancement and partial polarimetry," Appl. Opt. **51**(21), 5302–5309 (2012).
24. D. H. Goldstein, *Polarized Light* (CRC Press, 2017).
25. A. Peinado, A. Lizana, J. Vidal, C. Iemmi, and J. Campos, "Optimization and performance criteria of a Stokes polarimeter based on two variable retarders," Opt. Express **18**(10), 9815 (2010).
26. J. S. Tyo, "Design of optimal polarimeters: maximization of signal-to-noise ratio and minimization of systematic error," Appl. Opt. **41**(4), 619–630 (2002).
27. M. H. Smith, "Optimization of a dual-rotating-retarder Mueller matrix polarimeter," Appl. Opt. **41**(13), 2488–2493 (2002).

Optics EXPRESS

28. A. De Martino, E. Garcia-Caurel, B. Laude, and B. Drévillon, "General methods for optimized design and calibration of Mueller polarimeters," Thin Solid Films **455-456**, 112–119 (2004).
29. A. M. El-Saba, I. M. Elminyawi, and R. M. A. Azzam, "General analysis and optimization of the four-detector photopolarimeter," J. Opt. Soc. Am. A **5**(5), 681–689 (1988).
30. A. Ambirajan and D. C. L. Jr, "Optimum angles for a polarimeter: part I," Opt. Eng. **34**(6), 1651–1655 (1995).
31. S.-Y. Lu and R. A. Chipman, "Interpretation of Mueller matrices based on polar decomposition," J. Opt. Soc. Am. A **13**(5), 1106 (1996).
32. C. Heinrich, J. Rehbinder, and J. Zallat, "Revisiting the generalized polar decomposition of Mueller matrices," J. Opt. Soc. Am. A **37**(8), 1327 (2020).